

Experimental study of population inversion between excited states of Ar I in a recombining Ar plasma by He contact cooling

Katsuhiro Kano and Hiroshi Akatsuka*

Research Laboratory for Nuclear Reactors, Tokyo Institute of Technology, 2-12-1, O-Okayama, Meguro-ku, Tokyo 152-8550, Japan

(Received 14 June 2001; revised manuscript received 12 November 2001; published 29 April 2002)

An experiment of He gas contact for generating population inversion in a recombining Ar plasma jet is carried out. Population inversion between Ar I excited states $5s' \rightarrow 4p'[1/2]_1$ and $5s' \rightarrow 4p[3/2]_{1,2}$, $[5/2]_{2,3}$ is created by helium gas-contact cooling of electrons, whereas it is not created without gas contact. Ar I lines 1.14, 1.34, and 1.09 μm are strongly enhanced due to the He gas cooling. It is experimentally found that helium gas contact effectively lowers the electron temperature of the Ar plasma jet. The mechanisms giving rise to population inversion are discussed in terms of atomic collisional processes of the recombining plasma. The experimental results of electron temperature and population densities are discussed by a simple numerical analysis that we previously developed. It is shown that the experimental results are well explained by our modeling quantitatively for the case without gas contact, except that the agreement of number densities of lower lying nonlocal-thermodynamic-equilibrium levels is qualitative for the case with the gas contact.

DOI: 10.1103/PhysRevE.65.056404

PACS number(s): 52.20.-j, 34.90.+q, 52.25.Os, 52.59.Ye

I. INTRODUCTION

The authors have been studying fundamental spectroscopic characteristics of hydrogen and noble gas plasmas generated by a plasma jet apparatus [1]. These plasmas are in a typical recombining phase, and stationary population inversions of H I and He I have been observed by spectroscopic examinations [2–4]. On the other hand, no population inversion of Ar I was observed for the argon plasma in the same discharge apparatus. A collisional radiative model theoretically showed that the electron temperature should be sufficiently low in order to create population inversion in recombining plasmas [5]. We found that the electron temperature of the hydrogen and helium plasmas was about 0.1 eV or much lower and cold enough to make population inversion, whereas that of the argon plasma was about 0.5 eV, by spectroscopic measurement. It was supposed that the electron gas in the downstream region of the plasma jet becomes relaxed mainly by collisions with the residual gaseous molecules in the plasma jet chamber [4]. The authors consider that the result of the Ar plasma is attributed to the fact that the cross section of elastic collision between an electron and an argon atom is reduced owing to the Ramsauer effect in the energy range about 0.2–0.5 eV [6]. Consequently, electron temperature of the argon plasma does not become lower than 0.5 eV, and no population inversion occurs, whereas electron temperature of hydrogen and helium plasmas was found to be as low as 0.1 eV due to frequent collisions of electrons with residual gaseous molecules in the plasma expansion region, since they have no Ramsauer minimum in their elastic electron scattering cross sections.

In a TPD-I device at the National Institute for Fusion Science, population inversion of He II of the He plasma in contact with neutral helium gas [7–10] and that with neutral

hydrogen molecules [11] has been observed. The mechanisms leading to population inversion have been experimentally and numerically clarified [12–15]. We, therefore, expect that the population inversion of Ar I in our plasma jet apparatus should also be accomplished, if the electron temperature is appropriately decreased by gas-contact cooling like the TPD-I experiment, namely, making elastic collision frequent between electrons and gaseous target molecule with no Ramsauer minimum in its electron elastic collision cross section.

The authors have numerically investigated an effect of He gas-contact cooling of electrons on the generation of population inversion in the Ar plasma [16]. It was shown that the electron temperature of the Ar plasma was significantly decreased by gas-contact cooling, so that the population inversion of Ar I excited states $5s' \rightarrow 4p'[1/2]_1$ and $5s' \rightarrow 4p[3/2]_{1,2}$, $[5/2]_{2,3}$ was created. The objective of the present study is to demonstrate the effectiveness of the gas-contact cooling of electrons and to generate population inversion of Ar I experimentally. Another objective is to investigate the mechanism of the electron energy transfer in the recombining plasma jet.

II. EXPERIMENTAL SETUP

A. Expanding plasma jet apparatus

Figure 1 shows the schematic view of the plasma jet apparatus [1]. The apparatus is composed of a plasma generator, six magnetic coils, and a traversing mechanism for moving the optical fiber terminal assembly for spectroscopic examinations. These components are placed in a wind tunnel of 1.2 m in diameter and 2 m in length. The pressure in the wind tunnel is monitored by a Pirani gauge. The wind tunnel is evacuated with a 12 in. mechanical booster pump, where the ultimate pressure becomes as low as 0.40 Pa with its pumping rate 10 m^3/s .

Figure 2 shows the cross-sectional view of the electrodes for generating the plasma, and the expanding plasma through the nozzle. To specify the spatial position of the Ar plasma

*Email address: hakatsuk@nr.titech.ac.jp;
http://www.nr.titech.ac.jp/~hakatsuk/homeE.html

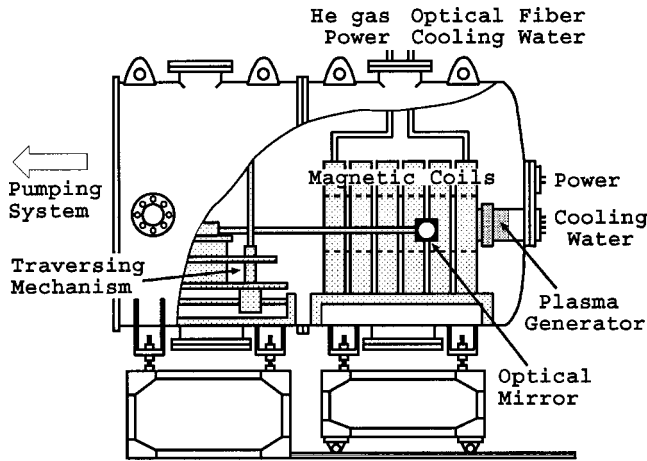


FIG. 1. Cross-sectional view of a plasma jet apparatus.

generated, the axial distance from the anode, z , is employed. The anode is made of copper, and has a nozzle of 1.2 mm diameter of a convergent throat shape. The cathode is made of a 2% thoriated tungsten rod of 3 mm in diameter. The argon plasma is generated by a dc arc discharge between the electrodes, and it expands after emerging from the nozzle on the anode. In the wind tunnel, six magnetic coils of 80 mm inner diameter are placed for confining the expanding plasma, with each gap distance of 1 cm. The strength of the magnetic field longitudinal to the center axis of the wind tunnel is about 0.15 T.

B. Spectroscopic measurements

Spectroscopic measurement was carried out for the plasma through the gaps between the magnetic coils at $z = 1, 8, 15,$ and 22 cm. In the present study, intensities of the line spectra listed in Table I were measured. To compare the results obtained by the numerical simulation [16], population densities of the levels defined in a collisional-radiative (CR)

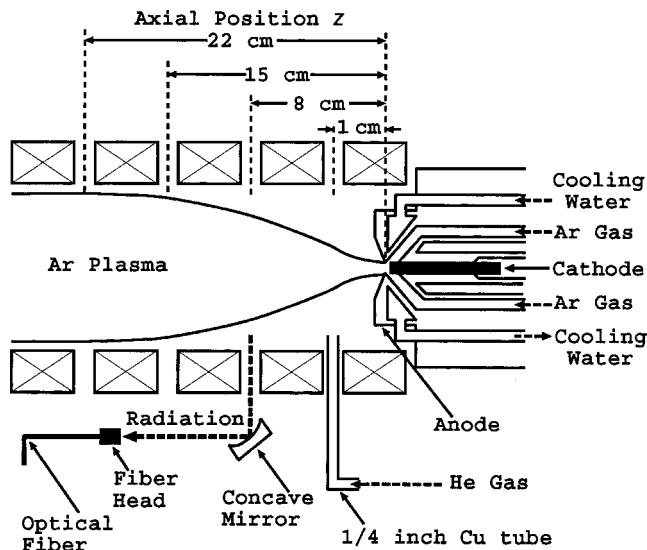


FIG. 2. Cross-sectional view of electrodes, magnetic coils, and argon plasma.

model [17] were chosen to be measured. An optical fiber assembly was employed to guide the radiation from the plasma to a monochromator system (JASCO, SS-50). The visible and infrared lines from the monochromator were detected by a photomultiplier tube (Hamamatsu, R374) and by a Ge photodiode (Hamamatsu, B3033-02), respectively. The signals from the photomultiplier tube or from the Ge photodiode were recorded by a computer. The sensitivity of the detection system was calibrated with a standard halogen lamp (Ushio Electric Corporation, JPD100V500WCS) and a white standard reflectance plate for a diffuse reflector.

C. Experimental conditions

A typical discharge condition is as follows: arc voltage $V_{\text{arc}} 18$ V, discharge current $I_{\text{arc}} 120$ A, pressure in the wind tunnel P_t without He injection 1.3 Pa.

As shown in Fig. 2, a stationary injection of neutral He gas into the Ar plasma is carried out at $z = 1$ cm in such a way that the Ar plasma is not perturbed. The pressure P_t when He gas is introduced is 5.5 Pa, which corresponds to the maximum He gas flow rate where the axial symmetry of the Ar plasma is not perturbed. The number density of He atom N_g at $z = 1$ cm was estimated from the conductance of the wind tunnel and from the capacity of the pumping system employed, on the assumption that the temperature of the injected He gas was 300 K, which showed N_g being $3.4 \times 10^{15} \text{ cm}^{-3}$. Experiments have been carried out for two cases: (A) the Ar plasma without He gas contact ($N_g = 0 \text{ cm}^{-3}$, hereafter called case A), and (B) the Ar plasma with He gas contact ($N_g = 3.4 \times 10^{15} \text{ cm}^{-3}$, hereafter called case B).

III. RESULTS AND DISCUSSION

A. Electron temperature

Electron temperature T_e was determined from population distributions of high-lying levels of the Boltzmann plots obtained by spectroscopic measurements, since it was already shown that these levels of recombining plasmas were in a state of PLTE (partially local thermodynamic equilibrium) [1–4]. Because the emission is observed along the direction perpendicular to the axis of the plasma jet and the Abel inversion is not applied, the electron temperature obtained by spectroscopic measurement approximately corresponds to mean value along the line of sight.

Figures 3(a) and 3(b) show the axial variation of the electron temperature of cases A and B, respectively. Electron temperature with gas contact (case B) becomes as cold as 0.44 eV at $z = 1$ cm, while that without gas contact (case A) remains 0.82 eV. This experimental result shows that rapid cooling of electrons is accomplished by the helium gas contact.

Because the line spectra arising from the transition between He I levels have never been observed in the present experiment, no He atoms prove to be excited by electron-impact collisions. Consequently, we can confirm that the decrease in electron energy when the neutral He gas is introduced is caused by elastic collisions (not by inelastic ones)

TABLE I. Basic spectroscopic data for the measured spectra. The number of energy levels (designations defined in the CR model) i , excitation energy E_i , transitions $j \rightarrow k (j > k)$ used for measurement of the population density of the i th level, corresponding wavelengths $\lambda_{j \rightarrow k}$, degeneracy of the k th level g_k and j th level g_j , transition probabilities $A_{j \rightarrow k}$.

Level i	Designation in CR model	E_i (eV)	Transition $j \rightarrow k$	$\lambda_{j \rightarrow k}$ (nm)	g_k	g_j	$A_{j \rightarrow k}$ (10^8 s^{-1})
6	$4p[1/2]_1$	12.907	$4p[1/2]_1 \rightarrow 4s[3/2]_2^o$	912.30	5	3	0.212
			$4p[1/2]_1 \rightarrow 4s[3/2]_1^o$	965.78	3	3	0.060
7	$4p[3/2]_{1,2}, [5/2]_{2,3}$	13.116	$4p[3/2]_2 \rightarrow 4s[3/2]_2^o$	763.51	5	5	0.274
8	$4p'[3/2]_{1,2}$	13.295	$4p'[3/2]_2 \rightarrow 4s[3/2]_1^o$	738.40	3	5	0.087
			$4p'[3/2]_1 \rightarrow 4s'[1/2]_0^o$	794.82	1	3	0.196
9	$4p'[1/2]_1$	13.328	$4p'[1/2]_1 \rightarrow 4s[3/2]_2^o$	696.54	5	3	0.067
10	$4p[1/2]_0$	13.273	$4p[1/2]_0 \rightarrow 4s[3/2]_1^o$	751.47	3	1	0.430
11	$4p'[1/2]_0$	13.480	$4p'[1/2]_0 \rightarrow 4s'[1/2]_1^o$	750.39	3	1	0.472
15	$5s'$	14.252	$5s'[1/2]_1^o \rightarrow 4p[3/2]_2$	1144.2	5	3	0.0156
			$5s'[1/2]_1^o \rightarrow 4p'[3/2]_2$	1300.8	5	3	0.100
16	$3d[3/2]_1, [5/2]_{2,3} + 5s$	14.090	$3d[5/2]_3^o \rightarrow 4p[5/2]_3$	1211.2	7	7	0.035
			$3d[5/2]_2^o \rightarrow 4p[5/2]_2$	1280.2	5	5	0.064
17	$3d'[3/2]_1$	14.304	$3d'[3/2]_1^o \rightarrow 4p'[3/2]_1$	1214.0	3	3	0.051
20	$4d + 6s$	14.792	$4d[7/2]_4^o \rightarrow 4p[5/2]_3$	737.21	7	9	0.020
			$4d[1/2]_0^o \rightarrow 4p[1/2]_1$	693.77	3	1	0.0321
26	$5d' + 7s'$	15.324	$5d'[5/2]_2^o \rightarrow 4p[3/2]_1$	573.95	3	5	0.0091
			$5d'[5/2]_3^o \rightarrow 4p'[3/2]_2$	614.54	5	7	0.0079
27	$5d + 7s$	15.153	$5d[7/2]_4^o \rightarrow 4p[5/2]_3$	603.21	7	9	0.0246
			$5d[7/2]_3^o \rightarrow 4p[5/2]_2$	604.32	5	7	0.0153
32	$6d' + 8s'$	15.520	$6d'[3/2]_2^o \rightarrow 4p[1/2]_1$	476.87	3	5	0.0090
			$6d'[5/2]_3^o \rightarrow 4p[5/2]_2$	511.82	5	7	0.0028
33	$6d + 8s$	15.347	$6d[1/2]_1^o \rightarrow 4p[1/2]_1$	516.23	3	3	0.0198
			$6d[5/2]_5^o \rightarrow 4p[5/2]_3$	544.22	7	7	0.00097
39	$7d + 9s$	15.460	$7d[7/2]_4^o \rightarrow 4p[5/2]_3$	522.13	7	9	0.0092
			$7d[3/2]_2^o \rightarrow 4p[1/2]_1$	487.63	3	5	0.0081

between electrons and He atoms. In addition, this result supports the effectiveness of the helium gas-contact cooling of electrons in the Ar plasma.

The decrease in T_e of case B from $z=0$ to $z=8$ cm becomes 0.48 eV, on the assumption that the electron temperature of case B at $z=0$ cm is close to that of case A at $z=1$ cm, that is, 0.82 eV. On the other hand, the decrease in T_e of case B from $z=8$ to $z=22$ cm is reduced to 0.04 eV. This reduction of electron cooling can be explained on the basis of energy balance equation for electrons [18]. As we specify in the following section, electron temperature is temporally traced by the energy balance equation describing the energy increase of electrons per unit time [19]. The equation is expressed as

$$\frac{dW_e}{dt} = R + Q, \quad (1)$$

where W_e is electron energy in a unit volume, i.e., $3N_e k_B T_e / 2$ (k_B being the Boltzmann's constant, and N_e being the electron density). The terms R and Q denote the energy transfer to free electrons due to elastic and inelastic collisions per unit time, respectively. And strictly speaking, concerning the term for elastic collisional processes, R , we

should take the effect of electron-He atom collisions (e -He) ε_{He} , electron-Ar collisions (e -Ar) ε_{Ar} , and electron-Ar⁺ (e -Ar⁺) elastic collisions $\varepsilon_{\text{Ar}^+}$ into account. In case B, the decrease in the electron energy is mainly attributed to the elastic collision processes between electrons and helium atoms ε_{He} . The effect of inelastic scattering process is also negligible as we showed in our previous work [16]. Therefore, the electron energy loss of case B can be estimated by the following equation [20]:

$$\frac{dW_e}{dt} \approx \varepsilon_{\text{He}} = - \frac{2m_e M_{\text{He}}}{(m_e + M_{\text{He}})^2} \frac{3}{2} k_B (T_e - T_g) \langle \nu_{\text{He}} \rangle N_e, \quad (2)$$

where m_e and M_{He} are the mass of an electron and a He atom, respectively; $\langle \nu_{\text{He}} \rangle$ is an effective collision frequency of electrons which collide with He atoms [21]; T_g is the He gas temperature. Since the collision frequency $\langle \nu_{\text{He}} \rangle$ in Eq. (2) is proportional to the He atom density N_g , rewriting Eq. (2) yields the simple expression

$$\frac{dW_e}{dt} \approx \varepsilon_{\text{He}} \propto - (T_e - T_g) N_g. \quad (3)$$

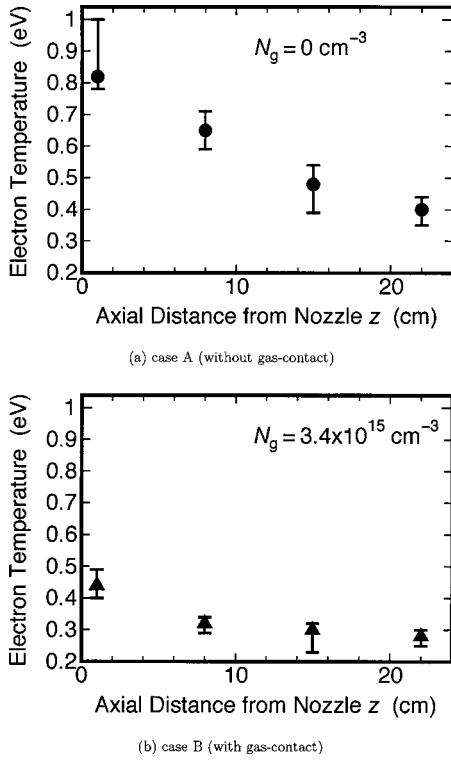


FIG. 3. Axial variation of electron temperature of (a) case A (without gas contact) and (b) case B (with gas contact).

This relationship shows that the energy transfer by the elastic collision of e -He is proportional both to the difference of the temperature ($T_e - T_g$) and to the density of He atom N_g . In the range of $z \geq 8$ cm, electron temperature of case B decreases as such that the effect of e -He elastic collision on the cooling of electrons becomes small. This is because the term ($T_e - T_g$) in Eq. (3) becomes smaller as T_e becomes close to T_g . Furthermore, because He atoms cannot be confined by the magnetic field and diffuse in the plasma chamber, the density of He atoms diminishes as the axial distance from the nozzle z increases. As a result, the effect of the gas contact on electron cooling is reduced, thus variation of T_e dwindles for the range of $z \geq 8$ cm. In other words, this result also shows the electron energy transfer arises from the e -He elastic collision, especially in the upstream region around $z \approx 1$ cm, where the density of He gas is sufficiently high, since it is just introduced into the plasma at this position.

B. Population density

Figures 4(a) and 4(b) show axial variation of the Boltzmann plots of Ar I for cases A and B, respectively. The basic spectroscopic data for the levels in the Boltzmann plots are summarized in Table I. In Fig. 4(b), since the population density at $z = 15$ cm is almost the same as that at $z = 22$ cm, the former is not presented. Besides, population densities of the levels $i = 6, 15, 16, 17$ are not shown for case A at any z or for case B at $z = 1$ cm, since the intensity of the corresponding line spectra in infrared region was too weak to observe.

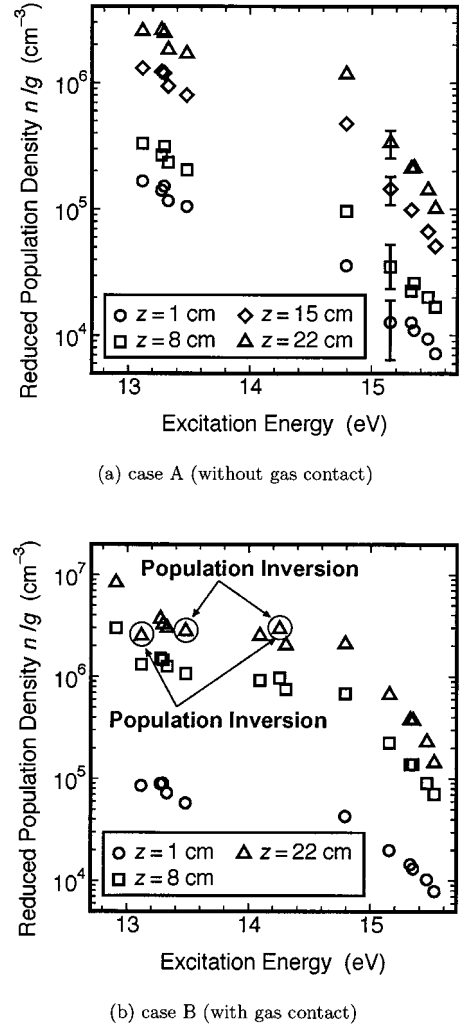


FIG. 4. Axial variation of reduced population density of (a) case A (without gas contact) and (b) case B (with gas contact).

It should be noted that the population densities at $z = 8$ cm of case B are about ten times higher than those of case A, which results from the difference in the electron temperature of each case, namely, whether the He gas is introduced or not. In case B, population inversions between Ar I excited states of $5s' \rightarrow 4p'[1/2]_1$ ($i = 15 \rightarrow 11$) and $5s' \rightarrow 4p[3/2]_{1,2}, [5/2]_{2,3}$ ($i = 15 \rightarrow 7$) are observed. The corresponding overpopulation densities $\Delta(N/g)$ are 1.3×10^5 and 4.3×10^5 cm^{-3} , respectively.

Figures 5(a) and 5(b) show the spectra of $5s'[1/2]_1^o \rightarrow 4p[3/2]_2$ transition for cases A and B at $z = 15$ cm, respectively. This transition is utilized for determining the population density of the level $5s'$ ($i = 15$), which corresponds to the upper level where population inversion occurs in case B, as previously mentioned. The intensity of the spectrum of case B is about ten times stronger than that of case A, since electrons accumulate at the level $i = 15$ through the rapid three-body recombination and electron-impact deexcitation, owing to decrease in T_e by gas contact in case B, which was confirmed by our previous calculation [16]. This directly succeeds in giving rise to the population inversion. It is concluded that the rapid cooling of electrons by the injection of

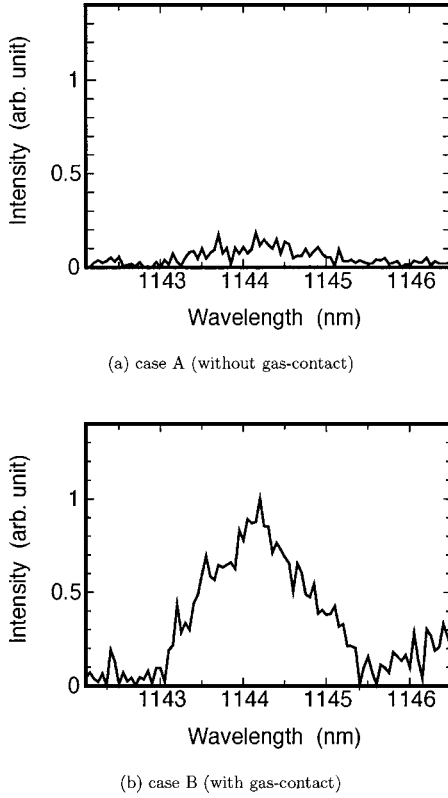


FIG. 5. Spectrum of $5s'[1/2]_1^0 \rightarrow 4p[3/2]_2$ transition for (a) case A (without gas contact) and (b) case B (with gas contact) at $z = 15$ cm.

He is effective for generating population inversion in the Ar plasma.

C. Discussion on the experimental results in terms of simple numerical modeling

1. Basic equations

In order to discuss the present experimental results quantitatively, it is worthwhile to review our numerical modeling of gas contact cooling of the argon plasma jet [16]. A numerical simulation is carried out under the following assumptions. A quasineutral Ar plasma penetrates into a homogeneous and spatially isotropic neutral He gas filled in the

wind tunnel. The list of symbols denoting the basic parameters used in the present study is given in Table II. The temperature of He gas T_g , is set to a fixed value, 300 K. Meanwhile, considering the present experimental conditions, we set N_g to 0 cm^{-3} for case A (without gas contact). For case B (with gas contact), it is quite difficult for us to measure the He number densities in the plasma expanding region experimentally. Therefore, to discuss the agreement of the numerical results with the present experimental ones, we assume three hypothetical He density profiles $N_g(t) \text{ cm}^{-3}$ as follows:

B1, the constant density profile,

$$N_g(t) = 3.4 \times 10^{15}, \quad (4)$$

B2, the decreasing density profile as the plasma comes downstream,

$$N_g(t) = \begin{cases} 1.0 \times 10^{16}(1 - v_z t)^2 + 1.0 \times 10^{15} & (0 < t \leq 1/v_z \text{ s}), \\ 1.0 \times 10^{15} & (t > 1/v_z \text{ s}), \end{cases} \quad (5)$$

and B3 the further decreasing profile,

$$N_g(t) = \begin{cases} 2.0 \times 10^{16}(1 - v_z t)^2 + 1.0 \times 10^{14} & (0 < t \leq 1/v_z \text{ s}), \\ 1.0 \times 10^{14} & (t > 1/v_z \text{ s}). \end{cases} \quad (6)$$

In the equations above, v_z (cm/s) is the longitudinal velocity of the plasma jet, which is assumed to be a constant value 1.6×10^5 cm/s and will be specified later in the following subsection. In the profile models B2 and B3, we assume that the He density N_g decreases till the plasma jet travels the distance of 1 cm, and that it becomes constant after that. This is because the contact helium gas is fed just near the nozzle, and its density will decrease due to expansion. These assumed He density profiles are shown in Fig. 6. Later, we will discuss the appropriateness of each assumption.

The temperature of Ar atoms T_a is set to be 1000 K. The ion temperature T_i is assumed to equal T_a . The pressure in the wind tunnel is 13.3 Pa, and the density of the ground state Ar atom N_1 is deduced from the discharge pressure and T_a using the law of ideal gases. The Ar plasma is assumed to drift toward the downstream direction in the wind tunnel with a constant velocity longitudinal to the center axis of the

TABLE II. List of symbols.

Symbol	Quantity	Numerical value (fixed)
T_g	He gas temperature	300 K
N_g	He gas density	0 cm^{-3} for case A $3.4 \times 10^{15} \text{ cm}^{-3}$ for case B
T_a	Ar gas temperature	1000 K
N_1	Density of ground state Ar atom	
T_i	Ion temperature	1000 K
T_e	Electron temperature	
N_e	Electron density	
T_{e0}	Initial electron temperature	0.82 eV
N_{e0}	Initial electron density	$1.0 \times 10^{13} \text{ cm}^{-3}$

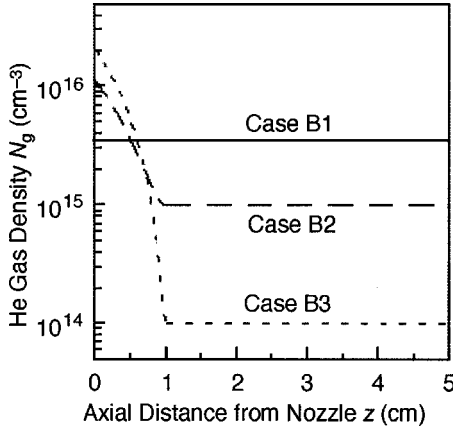


FIG. 6. Helium number density profile assumed in case B of the present simulation.

tunnel. Numerical calculation is carried out for the coordinate system drifting with the Ar plasma.

The basic equations for our calculation comprise (i) rate equations of excited states of Ar I, namely, a CR model for argon plasmas, (ii) an energy balance equation of electrons, and (iii) a conservation equation for electron number density.

The CR model utilized in the present study has been developed by Vlček [17]. The population densities of Ar I, N_i ($i=1,2,\dots,65$), are calculated from the following rate equations:

$$\frac{dN_i}{dt} = \sum_{j=1}^{65} a_{ji}N_j + \delta_i, \quad (7)$$

where a_{ji} and δ_i are the rate coefficients given by the following rate constants:

$$a_{ji} = \begin{cases} N_e C_{j,i} + N_1 K_{j,i} & (j < i), \\ N_e F_{j,i} + N_1 L_{j,i} + \Lambda_{j,i} A_{j,i} & (j > i), \\ - \left(N_e S_i + N_1 V_i + \sum_{l=1, l \neq i}^{65} a_{il} + D_i / \rho^2 + N_1^2 B_i \right) & (j = i), \end{cases}$$

and

$$\delta_i = N_e^2 (N_e O_i + N_1 W_i + \Lambda_i R_i),$$

where $C_{j,i}$ and $K_{j,i}$ are the rate coefficients for a $j \rightarrow i$ collisional excitation by electrons and by ground state atoms, respectively. $F_{j,i}$ and $L_{j,i}$ denote the rate coefficients for the $j \rightarrow i$ collisional deexcitations by their corresponding inverse processes, respectively. S_i and V_i are the rate coefficients for the collisional ionization of the level i by electrons and by ground state atoms, respectively, while O_i and W_i are the rate coefficients for the corresponding inverse three-body recombinations, and R_i is the radiative recombination rate coefficient. $A_{j,i}$ is the probability for a $j \rightarrow i$ spontaneous transition, $\Lambda_{j,i}$ and Λ_i are the optical escape factors bound-bound and bound-free transitions, respectively. B_i is the rate constant for the three-body collisions of metastables with the ground state atom. D_i and ρ are the diffusion coefficient for

metastable levels $i=2$ and 4, and the plasma radius, respectively. The levels taken into account in Eq. (7) are the same as those in the original CR model [17]. The appropriateness of the CR model has been confirmed by comparison with many experimental results [22–26]. With regard to the electron energy distribution function of this expanding plasma, we adopted Maxwellian distribution, which we experimentally confirmed by single probe examination.

Concerning the energy balance equation of electrons, we employ Eq. (1), since in the present simulation we have to treat the argon plasma jet without the gas contact (case A), where the elastic collisions between electrons and argon atoms as well as the inelastic collisions should be taken into account.

In the present study, all the He atoms are considered to be in the ground state, since the line spectra arising from the transition between He I levels have never been observed in the present experiment as previously mentioned. The initial electron temperature T_{e0} is set to 0.82 eV as was shown in Fig. 3(a). We also justifiably assume that T_a and T_g are kept constant, since the increase in these temperatures is negligibly small even if the total initial electron energy, $3N_{e0}k_B T_{e0}/2$, is transferred to Ar or He atoms. The initial electron number density N_{e0} is set to $1.0 \times 10^{13} \text{ cm}^{-3}$, according to our spectroscopic examinations at $z=1$ cm of case A.

We take the effect of electron-He atom (e -He), electron-Ar (e -Ar), and electron-Ar⁺ (e -Ar⁺) elastic collisions into account for elastic collisional processes, R , as was pointed out in the preceding subsection. The corresponding formulas for each process are described below.

With regard to the electron energy gain per unit time due to an e -He elastic collision, ε_{He} , we employ Eq. (2). For the effective collision frequency in Eq. (2), we adopted the effective collision frequency for Maxwellian electrons proposed by Baille *et al.* [27], which is given by

$$\langle \nu_{\text{He}} \rangle = \begin{cases} 3.53 \times 10^{-10} T_e^{0.562} N_g & (10^2 \text{ K} < T_e < 5 \times 10^3 \text{ K}), \\ 1.08 \times 10^{-9} T_e^{0.425} N_g & (3 \times 10^3 \text{ K} < T_e < 3 \times 10^4 \text{ K}), \end{cases} \quad (8)$$

where N_g is the number density of He atoms mixed in the Ar plasma. In Eq. (8), the units of T_e and N_g are K, and cm^{-3} , respectively.

Similar to Eq. (2), the increase in the electron energy due to e -Ar elastic collisions, ε_{Ar} , is expressed as

$$\varepsilon_{\text{Ar}} = - \frac{2m_e M_{\text{Ar}}}{(m_e + M_{\text{Ar}})^2} \frac{3}{2} k_B (T_e - T_a) \langle \nu_{\text{Ar}} \rangle N_e, \quad (9)$$

where M_{Ar} and $\langle \nu_{\text{Ar}} \rangle$ are the mass of an Ar atom, and the effective collision frequency of e -Ar elastic collisions [27]. They formulated the collision frequency $\langle \nu_{\text{Ar}} \rangle$ as follows [similar to Eq. (8)]:

$$\langle \nu_{\text{Ar}} \rangle = \begin{cases} 0.70 \times 10^{-8} T_e^{-0.315} N_{\text{Ar}} & (2.5 \times 10^2 \text{ K} < T_e < 6 \times 10^2 \text{ K}) \\ 2.58 \times 10^{-6} T_e^{-0.966} N_{\text{Ar}} + 2.25 \times 10^{-17} T_e^{2.29} N_{\text{Ar}} & (6 \times 10^2 \text{ K} < T_e < 1.4 \times 10^4 \text{ K}). \end{cases} \quad (10)$$

Additionally, the electron energy gain by the e -Ar⁺ elastic collision $\varepsilon_{\text{Ar}^+}$, is calculated by the equation

$$\varepsilon_{\text{Ar}^+} = - \frac{2m_e M_{\text{Ar}^+}}{(m_e + M_{\text{Ar}^+})^2} \frac{3}{2} k_B (T_e - T_i) \langle \nu_{\text{Ar}^+} \rangle N_e, \quad (11)$$

where M_{Ar^+} and $\langle \nu_{\text{Ar}^+} \rangle$ are the mass of an Ar ion, and the effective collision frequency of e -Ar⁺ elastic collisions [28], respectively.

As a result, the term R in Eq. (1) becomes

$$R = \varepsilon_{\text{He}} + \varepsilon_{\text{Ar}} + \varepsilon_{\text{Ar}^+}.$$

The term concerning inelastic collisions in Eq. (1), Q , is formulated under the following assumptions [19].

- (1) The energy transfer due to electron-impact transitions is exchanged with free electrons.
- (2) The energy required for ionization of Ar atoms is taken from free electrons. The energy of free electrons generated by an ionization process can be neglected. The electron energy released in the three-body electron recombination process is transferred to free electrons by the ionization energy of the level where the electron is captured (recombination heating).
- (3) The energy released in radiative transitions is not concerned with the increase in T_e .

Hence, the formulation of Q is expressed by

$$Q = - \left[\sum_{i=2}^{65} \sum_{j=1}^{i-1} (E_j - E_i) (C_{j,i} N_j - F_{i,j} N_i) + \sum_{j=1}^{65} E_j S_j N_j - N_e^2 \sum_{j=1}^{65} E_j O_j + \frac{3}{2} k_B T_e N_e \sum_{j=1}^{65} R_j + N_e N_1 \sum_{j=1}^{65} W_j E_j \right] N_e, \quad (12)$$

where E_i is the ionization potential of the level i of the Ar atom.

The equation for conservation of electron number density is expressed by a balance equation for ionization and recombination on the basis of the CR model,

$$\frac{dN_e}{dt} = \sum_{j=1}^{65} [(N_j S_j + N_j V_j) N_e - (N_e O_j + N_1 W_j + R_j) N_e^2]. \quad (13)$$

The outline of the computational procedure is as follows. The initial condition for population densities of Ar atom N_i ($i=2,3,\dots,65$), is given by a steady-state solution of the CR model as functions of initial electron temperature T_{e0} and density N_{e0} , and a set of input parameters. Then, time evolutions of T_e , N_e , and N_i are calculated as a function of time t through temporal integration of Eqs. (1), (7), and (13). Due to the limitation of the capability of our work station, we

stopped the simulation at the time 9.4×10^{-5} s, which was correspondent to the movement of the plasma jet from $z=0$ cm to $z=15$ cm.

2. Numerical results and comparison

In order to compare the numerical results with the present experimental ones, we need to know the longitudinal component of velocity of the plasma jet v_z , which was difficult for us to measure in the experiments. Here, we refer that of the hydrogen plasma jet in the present apparatus, which was measured from the Doppler shift of H α line [2], where it was shown that v_z of the hydrogen plasma jet was about 1×10^6 cm/s. It was considered that the dissociation degree of hydrogen was almost unity due to the high initial gas temperature of the arc plasma jet. If we assume that the Mach number of the argon plasma jet should be approximately equal to that of the hydrogen plasma jet, we can roughly estimate the longitudinal velocity of the argon plasma jet to be

$$\frac{v_z(\text{Ar})}{v_z(\text{H})} = \sqrt{\frac{\gamma(\text{Ar}) M_{\text{H}}}{\gamma(\text{H}) M_{\text{Ar}}}}, \quad (14)$$

where γ denotes the specific-heat ratio and M_{H} the mass of the hydrogen atom. In consequence, the value of v_z of the argon plasma jet is estimated at 1.6×10^5 cm/s. For a simple comparison, we also assume that the argon plasma drifts downstream at the uniform velocity 1.6×10^5 cm/s. This enables us to compare the experimental results with the calculation, by regarding that the longitudinal distance z corresponds to $v_z t$.

As a result, Figs. 7(a) and 7(b) show the calculated values of T_e for case A (without the gas contact) and for cases B1, B2, and B3 (with the gas contact), respectively, together with their corresponding experimental results. It is found that the calculated electron temperature agrees well with our experimental results for case A. Although we made many assumptions in the course of our formulation, they are considered to be basically sufficient for quantitative numerical analysis for case A, namely, without gas contact.

Concerning electron temperature for cases with gas contact, the agreement of the case B1 (constant density) is the poorest of the three. Of course, this is attributed to the unjustified assumption of the helium density profile. The helium density should become smaller as the plasma flows to the downstream region. The density for the case B1 was calculated as such at the nozzle from experimentally observed pressure together with conditions of the vacuum system. However, the effect of the helium contact cooling of case B1 is still insufficient. As we increase the value of helium density assumed at $z=0$, the agreement becomes better. At $z=1$ cm, numerical results of case B3 show the best

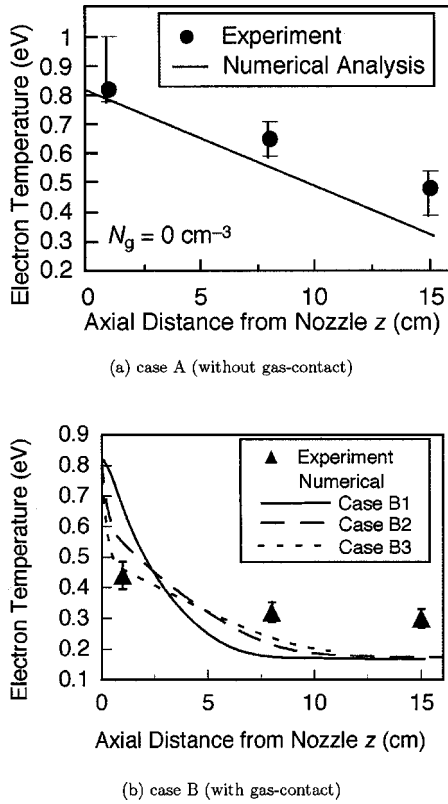


FIG. 7. Comparison of the electron temperature measured in the present experiments with that calculated by our simple numerical analysis. (a) case A (without gas contact) and (b) case B (with gas contact).

agreement of the three assumed cases. Therefore, it is concluded that the value of helium density just near the nozzle should be about $(1-2) \times 10^{16} \text{ cm}^{-3}$.

On the other hand, for the downstream region ($z \geq 8 \text{ cm}$), the agreement of the case B1 is the worst again, where the effect of gas-contact cooling becomes too strong to reproduce the experimental result. In the downstream region, the helium gas density should become lower, at least like the case B2. Nevertheless, the electron temperature calculated for the case B2 is still lower than that measured experimentally. It should be noted that the agreement is not much improved even if we assume lower helium density there. As a matter of fact, the helium density of the case B3 at $z \geq 1 \text{ cm}$ is considered to be unrealistically low, if we consider the conductance of our vacuum system. When we assume that the helium density should be $1 \times 10^{15} \text{ cm}^{-3}$ (case B2) in this region, the effect of helium contact cooling becomes less remarkable than that by ion-electron collisions. Therefore, the helium density at $z \geq 8 \text{ cm}$ is estimated to be of the order of $1 \times 10^{15} \text{ cm}^{-3}$.

Of course, the effect of the gas-contact cooling should be evaluated quantitatively. It is quite suggestive for us to discuss the effect on energy loss of electrons by the helium gas contact in terms of elastic collisional processes. Table III shows the energy loss of electrons per unit volume per unit time due to elastic collisions with helium atoms ε_{He} , with argon atoms ε_{Ar} , and with argon ions $\varepsilon_{\text{Ar}^+}$, by applying Eqs.

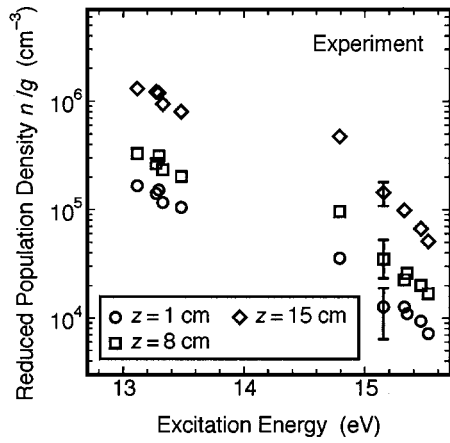
TABLE III. Energy loss of electrons per unit time per unit volume by elastic collisions with helium atoms ε_{He} , with argon atoms ε_{Ar} , and with argon ions $\varepsilon_{\text{Ar}^+}$, calculated by Eqs. (2), (9), and (11), respectively, for case A (without helium gas contact) and for case B2 (with helium gas contact). The unit of ε is $\text{J cm}^{-3} \text{ s}^{-1}$. Read $1.4 [-3]$ as 1.4×10^{-3} , etc.

	$z=0 \text{ cm}$	$z=1 \text{ cm}$	$z=8 \text{ cm}$	$z=15 \text{ cm}$
(a) Case A (without gas contact)				
$ \varepsilon_{\text{He}} $	0.0 [+0]	0.0 [+0]	0.0 [+0]	0.0 [+0]
$ \varepsilon_{\text{Ar}} $	1.5 [-3]	1.4 [-3]	6.6 [-4]	2.4 [-4]
$ \varepsilon_{\text{Ar}^+} $	1.5 [-2]	1.5 [-2]	1.6 [-2]	1.6 [-2]
(b) Case B2 (with gas contact)				
$ \varepsilon_{\text{He}} $	2.8 [-1]	1.5 [-2]	3.6 [-3]	2.6 [-3]
$ \varepsilon_{\text{Ar}} $	1.5 [-3]	2.2 [-4]	2.2 [-5]	1.4 [-5]
$ \varepsilon_{\text{Ar}^+} $	1.7 [-2]	1.6 [-2]	1.5 [-2]	2.4 [-2]

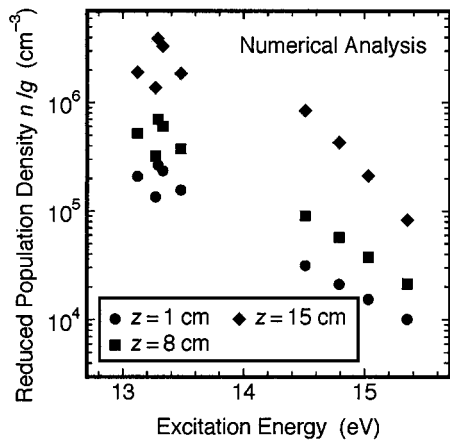
(2), (9), and (11), respectively, calculated numerically. As was expected, irrespective of the helium contact, the effects of the elastic collisions with argon atoms are much smaller than with argon ions, which results from the Ramsauer minimum of the electron scattering cross section of an argon atom. It is also found that the helium contact cooling is very effective just after the plasma jet comes out of the nozzle ($z=0 \text{ cm}$). Without helium contact, elastic collisions with argon ions are the most predominant processes for energy loss of electrons.

Generally, the gas contact effect becomes more essential as the difference in the temperature ($T_e - T_g$) becomes larger. In addition, the collision frequencies of electrons with neutral species ($\langle \nu_{\text{He}} \rangle$ and $\langle \nu_{\text{Ar}} \rangle$) also increase as T_e increases in the present electron temperature range. Meanwhile, since the ion-electron collision frequency $\langle \nu_{\text{Ar}^+} \rangle$ is approximately proportional to $T_e^{-1.5}$, the electron energy loss by ion-electron collisions is almost constant in the plasma jet, and is hardly affected by the helium contact itself. It means that the ratio $|\varepsilon_{\text{He}}|/|\varepsilon_{\text{Ar}^+}|$ increases as T_e increases, and consequently, the helium gas-contact cooling becomes more dominant in the high- T_e region than in the low- T_e region. Therefore, T_e experimentally observed at $z=1 \text{ cm}$ of case B becomes much lower than that of case A, which shows the effectiveness of helium gas contact in the upstream region of the plasma jet.

Concerning the effect of inelastic collisions Q , we can understand the qualitative behavior of the electron energy loss by inelastic collisions. Generally, the sign of R is negative according to the definition of ε [see Eqs. (2), (9), and (11)], since electrons lose their energy at elastic collisions. On the other hand, our previous numerical study shows that the sign of Q becomes positive, because the released energy at dominant three-body recombinations is deposited to free electrons due to recombination heating [16]. It is found that the energy gain by inelastic collision almost cancels the energy loss by elastic collisions when $T_e \leq 0.3 \text{ eV}$. For this reason, electron temperature of cases B1–B3 does not decrease at $z \geq 10 \text{ cm}$. Meanwhile, electron temperature of case A still decreases even at $z=15 \text{ cm}$, because the three-body



(a) Experimental results



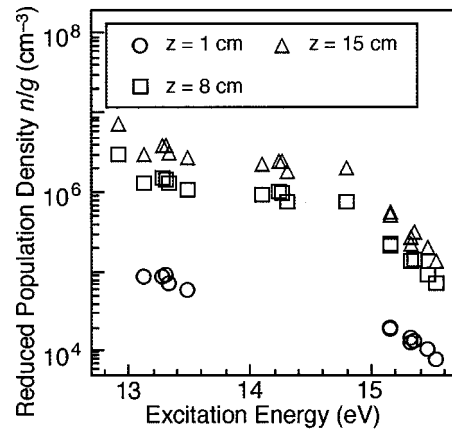
(b) Numerical results

FIG. 8. Comparison of the reduced population densities of some excited states of Ar I in the present experiments with those calculated by our simple numerical analysis without gas contact (case A). (a) experimental results and (b) numerical results.

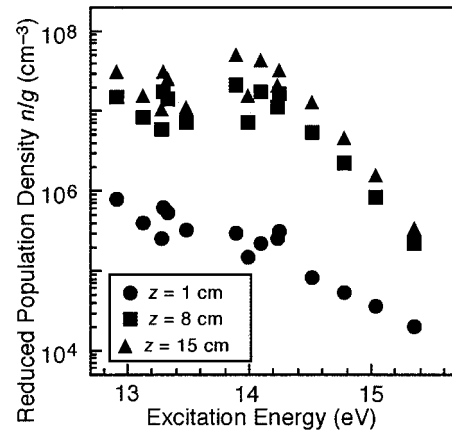
recombinations are still not dominant due to high T_e , which results in the relationship $R + Q < 0$.

Figures 8(a) and 8(b) show the experimental and numerical results of reduced population densities N_i/g_i , respectively, of some excited states of Ar I without gas contact (case A). It is seen that the present numerical results approximately reproduce the experimental ones. It is confirmed that the present modeling is quantitatively sufficient to simulate the population densities as well as the electron temperature of the argon plasma jet for case A (without gas contact).

On the other hand, Figs. 9(a) and 9(b) show the experimental and numerical results, respectively, with gas contact (case B2). When we compare Figs. 9(a) and 9(b), it is seen that the agreement is satisfactory for the highly excited states whose excitation energy is more than 14.7 eV. With regard to lower lying excited states, however, disagreement is remarkable, especially, at $z=8$ and 15 cm. This is because the numerical result of the electron temperature, shown in Fig. 7(b), was much lower than the experimental results for case B2. Of course, the agreement for the He density assumption



(a) Experimental results



(b) Numerical results

FIG. 9. Comparison of the reduced population densities of some excited states of Ar I in the present experiments with those calculated by our simple numerical analysis with gas contact (case B2). (a) experimental results and (b) numerical results.

of case B2 is much more improved than that of the case B1. However, the agreement was not improved even when we assumed the density profile to be that of case B3, where He number density was unrealistically low.

Generally, the population densities of the excited states of recombining plasmas increase as the electron temperature becomes lower, since the rates of the electron three-body recombination and the electron impact deexcitation become enhanced. Without gas contact, the numerical results of population densities approximately agree with the experimental ones, because the value of the electron temperature is still as high as about 0.5 eV, and the three-body recombination and following electron impact deexcitation are not dominant. It is considered that the lower lying excited states of Ar I without gas contact are almost in the state of PLTE, due to slow relaxation of electrons. On the other hand, with the gas contact, since the degree of nonequilibrium becomes enhanced, the calculated number densities of lower excited states become higher than those observed experimentally. It is considered that these levels whose energy is less than 14.7 eV are not in the state of PLTE. It should be noted that even

in such a situation, the number densities of PLTE levels (highly excited states) are well described by the present simple numerical model.

It is considered that this disagreement shows the limit of validity of the present numerical model, where the longitudinal velocity of the plasma jet is constant, and the plasma flow is treated as a one-dimensional problem. In order to improve the numerical simulation, we should understand not only the fluid dynamic behavior of helium gas introduced into the plasma chamber but also that of the plasma jet itself, which is beyond the scope of the present study.

IV. CONCLUSION

The experiment of He gas contact for cooling of electrons in the recombining Ar plasma jet was demonstrated. Without helium gas contact, electron temperature of the Ar plasma decreased slowly, and in consequence, no population inversion was found in excited states of Ar I. By the helium contact cooling, the electron temperature decreased very rapidly as the plasma jet came downstream, and population inversion was created. Population inversion between Ar I excited states of $5s' \rightarrow 4p'[1/2]_1$ and $5s' \rightarrow 4p[3/2]_{1,2}, [5/2]_{2,3}$ occurred through rapid electron cooling by elastic collision between electrons and He atoms. This is attributed to the difference in the electron elastic collision cross section between helium and argon. The electron collision cross section of Ar has its

minimum around electron energy 0.2–0.5 eV due to the Ramsauer effect, which is not the case with helium. Therefore, it was confirmed that the electron energy was transferred by the elastic collisions of electrons to the neutral gas molecules in the recombining plasma jet. In addition to the experiments, numerical calculation was carried out to understand the temporal variation of electron temperature and of population densities of excited states of argon atoms. Consequently, it was found that the numerical methods that we previously proposed quantitatively explained the variation of the electron temperature and population densities for the case without helium contact cooling. On the other hand, for the case with gas contact, three hypothetical He number density profiles were assumed and we confirmed the agreement of electron temperature and number densities of PLTE levels between calculations and experiments. However, the agreement of the population densities of lower lying excited levels in the state of non-PLTE was rather qualitative, due to the simplified modeling of the fluid dynamics of the helium gas introduced into the argon plasma as well as those of the plasma jet itself.

ACKNOWLEDGMENT

The authors thank Professor J. Vlček of the University of West Bohemia for allowing us to use his excellent argon CR model code.

-
- [1] H. Akatsuka and M. Suzuki, *Rev. Sci. Instrum.* **64**, 1734 (1993).
 - [2] H. Akatsuka and M. Suzuki, *Phys. Rev. E* **49**, 1534 (1994).
 - [3] H. Akatsuka and M. Suzuki, *Contrib. Plasma Phys.* **34**, 539 (1994).
 - [4] H. Akatsuka and M. Suzuki, *Plasma Sources Sci. Technol.* **4**, 125 (1995).
 - [5] T. Fujimoto, *J. Phys. Soc. Jpn.* **47**, 265 (1979); **47**, 273 (1979); **49**, 1561 (1980); **49**, 1569 (1980); **54**, 2905 (1985).
 - [6] A. W. Yau, R. P. McEachran, and A. D. Stauffer, *J. Phys. B* **13**, 377 (1980).
 - [7] M. Otsuka, R. Ikee, and K. Ishii, *J. Quant. Spectrosc. Radiat. Transf.* **15**, 995 (1975).
 - [8] M. Otsuka, R. Ikee, and K. Ishii, *J. Quant. Spectrosc. Radiat. Transf.* **21**, 41 (1975).
 - [9] K. Sato, M. Shiho, M. Hosokawa, H. Sugawara, T. Oda, and T. Sasaki, *Phys. Rev. Lett.* **39**, 1074 (1977).
 - [10] K. Sato, *J. Phys. Soc. Jpn.* **43**, 1027 (1977).
 - [11] T. Oda *et al.*, *Short-Wavelength Lasers and Their Applications*, edited by C. Yamanaka (Springer-Verlag, Berlin, 1988).
 - [12] T. Oda, K. Sato, S. Namba, S. Kusakabe, K. Takahara, H. Tawara, T. Katsuta, K. Takiyama, and U. Furukane, *J. Nucl. Mater.* **241–243**, 1238 (1997).
 - [13] T. Oda, U. Furukane, K. Takiyama, K. Sato, and H. Tawara, *Fusion Eng. Des.* **34–35**, 773 (1997).
 - [14] S. Namba, S. Kusakabe, K. Takahara, K. Sato, T. Katsuta, and T. Oda, *Fusion Eng. Des.* **34–35**, 777 (1997).
 - [15] S. Namba, I. Nomura, K. Iwasaki, K. Takiyama, U. Furukane, T. Oda, and K. Sato, *J. Nucl. Mater.* **266–269**, 1157 (1999).
 - [16] K. Kano and H. Akatsuka, *Jpn. J. Appl. Phys., Part 1* **40**, 4701 (2001).
 - [17] J. Vlček, *J. Phys. D* **22**, 623 (1989).
 - [18] U. Furukane and T. Oda, *Z. Naturforsch. Teil A* **39A**, 132 (1984).
 - [19] U. Furukane, K. Sato, and T. Oda, *J. Phys. D* **22**, 390 (1989).
 - [20] A. Gilardini, *Low Energy Electron Collisions in Gases*, edited by S. C. Brown (Wiley, New York, 1972).
 - [21] Y. Itikawa, *Phys. Fluids* **16**, 831 (1973).
 - [22] J. Vlček and V. Pelikán, *J. Phys. D* **22**, 632 (1989).
 - [23] J. Vlček and V. Pelikán, *J. Phys. D* **23**, 526 (1990).
 - [24] J. Vlček and V. Pelikán, *J. Phys. D* **24**, 309 (1991).
 - [25] J. Vlček and V. Pelikán, *Spectrochim. Acta, Part B* **47**, 681 (1992).
 - [26] A. Bogaerts, R. Gijbels, and J. Vlček, *Spectrochim. Acta, Part B* **53**, 1517 (1998).
 - [27] P. Baille, J. S. Chang, A. Claude, R. M. Hobson, G. L. Ogram, and A. W. Yau, *J. Phys. B* **14**, 1485 (1981).
 - [28] R. Deloche, P. Monchicourt, M. Cheret, and F. Lambert, *Phys. Rev. A* **13**, 1140 (1976).